JOURNAL OF MATERIALS SCIENCE 25 (1990) 3008–3016

The thermal stability of Ni–11 wt % P metallic glass

J. H. HAMLYN-HARRIS, D. H. StJOHN*
Department of Mining and Metallurgical Engineering, University of Queensland, St. Lucia, 4067 Queensland, Australia

D. K. SOOD
Microelectronics Technology Centre, Royal Melbourne Institute of Technology, 124 La Trobe St., Melbourne 3000, Victoria, Australia

A study of the crystallization of the metallic glass $Ni_{81}P_{19}$ was undertaken. A portion of the crystallization time–temperature–transformation curve was determined and compared with curves published by other authors. The composition and structure of the as-received metallic glass was determined. Crystallization kinetics of the glass and activation energy data were determined. Crystallization of the glass involved nucleation and growth of the crystalline phase from both the surface of quenched-in crystals and the bulk of the material. The activation energies obtained were similar for incubation, nucleation and growth. This along with supporting experimental evidence suggests that there is no activation barrier to nucleation and that all stages of crystallization are controlled by diffusion.

1. Introduction

Metallic glasses are metastable, and thermal activation over a suitable time can result in sufficient crystallization of the alloy to cause a change of properties. It is therefore desirable to understand the thermal stability of a metallic glass in order to estimate its useful life at a particular temperature.

Thermal stability studies can be carried out on metallic glasses in a number of ways. Thermal analysis methods such as differential thermal analysis (DTA) and differential scanning calorimetry (DSC), and microscopic methods such as optical and electron microscopy are most common [1–4]. Other methods include electrical resistivity studies, nuclear magnetic resonance (NMR) and elasticity measurements [5].

A commonly quoted measure of thermal stability is the crystallization temperature which is obtained at different heating rates by different workers [6–12]. Since crystallization is a diffusion-controlled reaction, crystallization time (or heating rate) is as important as temperature, and needs to be reported along with the corresponding temperature. Such data lead to the construction of time–temperature–transformation (TTT) curves allowing the determination of crystallization temperature for a range of annealing times and heating rates. A knowledge of the alloy's TTT curve is important to gain a complete understanding of its thermal stability, e.g. the activation energy (and appropriate pre-exponential factor) can be calculated, enabling the prediction of crystallization times at any temperature.

Several transition metal–metalloid (TM–M) type metallic glasses have been extensively studied [13]. The Ni–P system has been studied by several workers. Many studies [14–16] have been on Ni–P made by electrodeposition rather than rapid solidification. The Ni–P system forms a simple binary eutectic at 11 wt % P (19 at % P), making it a suitable material for the formation of a TM–M glass.

Naka *et al.* [10] calculated the curved portion (or nose) of the TTT curve for a number of transition metal–phosphorus glasses including Ni–P from a theoretically derived equation. These authors appear to have considered this TTT curve only as a means of determining the critical cooling rate for amorphization, since their crystallization study does not include crystallization time data with crystallization temperatures. Bergmann and Fritsch [17] determined a TTT curve for $Ni_{81}P_{19}$, using a combination of DTA, DSC and optical metallography techniques. They also measured the distribution of quenched-in crystals.

Naka *et al.* [10] studied the crystallization behaviour of the same alloy, in their broad study mentioned above, and reported metastable phases which were called Crys I and Crys II before the equilibrium Ni_3P phase was reached. Thermal stability data were incomplete, however, as no crystallization times were reported. T_c was stated to be 601 K.

Criado *et al.* [4] studied the crystallization of Ni–P metallic glass using DSC and X-ray diffraction (XRD) techniques and reported that the amorphous phase breaks down to form nickel and Ni_3P, contrary to previous reports [18–21] of a number of intermediate crystallization products. They also calculated the

Present address: CRA Advanced Technical Development, Unit 8, R & D Building, 1, Sarich Way, Tech Park, Bentley O.W.A. 6107, Australia.

0022–2461/90 $03.00 + .12

activation energy for crystallization for the glass to be $283 \pm 5\,kJ\,mol^{-1}$, but did not quote a pre-exponential factor.

Bakonyi *et al.* [14] studied the crystallization of electrodeposited Ni–P alloys of different compositions using DSC and TEM. DSC results indicated a two-stage crystallization process for hypoeutectic alloys consisting of primary nickel precipitates followed by Ni_3P and nickel. Hypereutectic alloys crystallized first to Ni_5P_2 and nickel, followed by recrystallization to Ni_3P. The authors suggest that the reason Ni_5P_2 is metastable in this case is because the compound is actually a supersaturated solid solution containing excess nickel. The crystallization temperature was about 625 K at a heating rate of $10\,K\,min^{-1}$ for the eutectic alloy.

Pitterman and Ripper [15] studied similar alloys by high-energy electron diffraction and found almost identical crystallization behaviour in hypoeutectic alloys. Hypereutectic alloys crystallized to Ni_3P and Ni_5P_2 phases.

Ding *et al.* [16] studied crystallization and hydrogen embrittlement of electrodeposited $Ni_{83.3}P_{16.7}$ and found crystallization to occur at 270° C after 30 min annealing. Detection was by XRD and transmission electron microscopy (TEM). Irradiation with a 100 kV electron beam was sufficient to re-amorphize the alloy.

The nickel–phosphorus system was chosen for the present study as part of a broader investigation comparing the thermal stability of amorphous alloys produced by planar flow casting and ion-implantation. The surface alloys made by ion-implantation were studied by transmission electron microscopy [22]. Thermal stability was assessed by TTT curve, activation energies and crystallization kinetics.

This paper presents the results of a crystallization study of the metallic glass $Ni_{81}P_{19}$. The experimental methods used to determine TTT curves, kinetics and activation data are described, followed by a characterization of the as-received metallic glass. Experimental results for crystallization behaviour follow. The natures of the observed nucleation and growth of the crystalline phases are discussed and possible explanations of the observed behaviour are presented.

2. Experimental methods

The metallic glass (of composition Ni–11 wt % P–0.1 wt % C–0.2 wt % Fe, code MBF60), was obtained from Nippon Amorphous Metals, Japan. The glass was in the form of ribbon with dimensions 40 μm thick and 25 mm wide.

The thermal stability of the metallic glass was determined by a number of methods, depending on the annealing times. For very short times such as 2 min or less, continuous-heating DTA was performed in a Rigaku DTA machine. Evaluations of crystallization temperature were performed at seven heating rates in air and in argon. It was found that in an air atmosphere, significant oxidation occurred on the specimens, and crystallization temperatures were lower by about 10° C. Because of this only TTT data determined from tests in an argon atmosphere were used. T_c values were determined in the range of 320 to 390° C.

For times ranging from 10 to 400 min, DTA was performed isothermally in a controlled-atmosphere tube furnace fitted with reference and specimen thermocouples. An argon atmosphere was used for all tests, though at lower temperatures some tests were conducted in air. It was found that at temperatures below about 270° C, an air atmosphere did not cause significant oxidation and crystallization times were not affected.

For times ranging from 40 min to several months, specimens were annealed in air-recirculating furnaces and optical metallography was used to observe the microstructure.

Most crystallization times were corrected for the effect of the heating time required before a stable temperature was reached. The corrections were made by an iterative method of estimating the crystallization time–temperature function from experimental data. This was then used to calculate the effects on the experimentally determined crystallization times of either

(a) warm-up time (isothermal DTA tests), or

(b) constant heating rate (conventional DTA).

Times were thus corrected and the process repeated until the corrections became insignificant. Further details and the programs used are available in published work [22, 23] or from the first author.

The crystal growth rates at different temperatures were measured during crystallization from micrographs taken on an optical microscope and micrographs taken during crystallization in the hot-stage TEM.

Optical metallography was used to study the growth kinetics of the glasses crystallized in air-recirculating furnaces. These treatments lent themselves to periodic interruption without any appreciable errors, because the time taken for the specimens to attain the required temperature (typically 1 min) was insignificant compared to the total annealing time. Parts of the same ribbon were periodically removed from the furnace and mounted in cold-setting Epimount resin compound (Epirez Australia Pty Ltd), polished and etched in Fry's reagent to reveal the quenched-in crystals and crystallization product. Growth rates were determined from the slope of plots of precipitate section size against time.

For shorter times, hot-stage TEM was used. This gave an opportunity for a few estimations of crystallization time while growth rates were being measured. Samples of metallic glass were thinned for TEM in a Tenupol apparatus using a solution of 40% perchloric acid, 40% methanol and 20% water at 4 to 12° C at 20 V. Specimens were then heated in a Jeol EM-SHTH double-tilt hot stage to a pre-determined temperature, and the crystallization process was observed and photographed in a Jeol-100CX electron microscope operating at 100 kV. These photographs were used to determine growth rates. The time taken for crystallization was also recorded. Times were recorded for 1%, 50% and in some cases 100% of the electron-transparent (and amorphous) areas to crystallize.

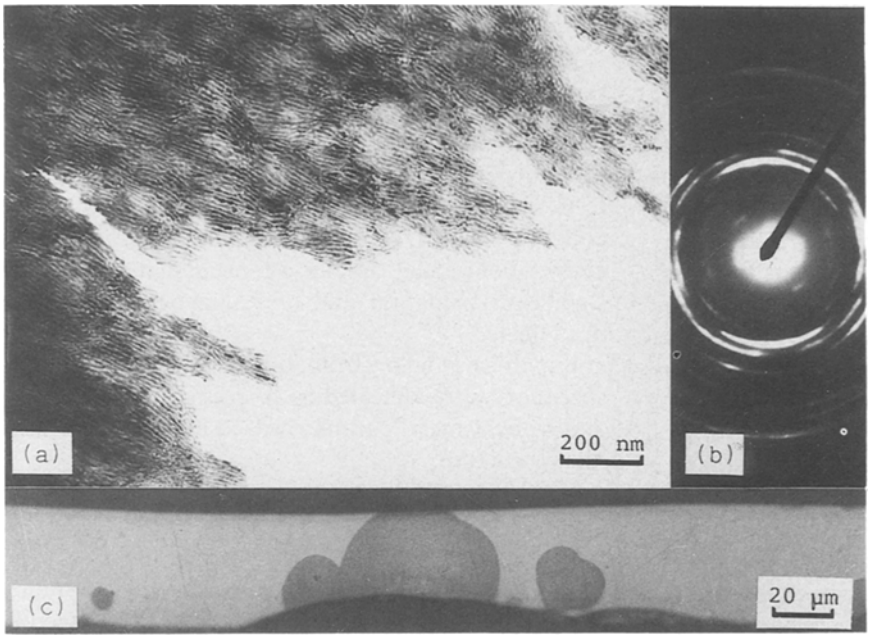

Figure 1 Quenched-in crystals in the as-received Ni–P metallic glass: (a) TEM micrograph (b) electron diffraction pattern (c) optical micrograph.

3. Characterization of material

The composition of the as-received metallic glass was checked using energy-dispersive spectroscopy (EDS) in a scanning electron microscope (SEM). The results compared well with the published analysis of the manufacturer, the only difference being 0.2 wt % Fe detected in addition to the already-stated elements.

The as-received glass was found to contain quenched-in grains of lamellar Ni–Ni_3P eutectic ranging in size from less than 1 to 40 μm, and growing from the dull (roller) side of the ribbon (Fig. 1). The phases were indentified as nickel (fcc) and Ni_3P (bct) by electron diffraction and XRD.

The compositions of both crystalline and amorphous structures were analysed. The composition of the quenched-in crystals was not found to be significantly different from that of the amorphus areas, indicating that no solute rejection occurred during solidification and the original crystallization mode was purely eutectic.

The inter-lamellar spacing of the eutectic was found to be in the range of 15 to 25 nm, as measured by TEM.

The quenched-in crystals were considered to have formed on the roller side of the ribbon in regions of lower cooling rate. These regions could be caused by the entrapment of gas bubbles and/or foreign matter during the melt spinning process [24], which would act as local thermal insulators lowering the local cooling rate and displacing metal in the melt puddle (causing the roller side of the ribbon to be uneven).

The number density of quenched-in crystals was estimated by counting the number of eutectoid grains intersecting the surface after partial crystallization, assuming an average diameter of 4 μm. This gave a number density of 5×10^{15} crystals m^{-3}. This is similar to the 1×10^{15} crystals m^{-3} reported in a partially crystallized $Co_{70}B_{30}$ metallic glass by Koster [25].

Quenched-in crystals were observed with diameters up to 40 μm. Morris [26] determined the empirical relationship between cooling rate and microcrystallite size (assumed to be the equivalent of eutectic colony size) for a number of alloys, including nickel based alloys, as

$$D = 1090T^{-0.45} \quad (1)$$

where D = grain size in micrometers and T = cooling rate in K sec^{-1}. Using this equation and the diameters of the quenched-in crystals, the cooling rates in the melt spinning process can be determined. Cooling rates have been calculated from this equation for a range of sizes. They varied from 4.5×10^3 K sec^{-1} for the largest 40 μm crystals to 2.6×10^7 K sec^{-1} for crystals of 0.5 μm diameter.

4. Results and discussion

4.1. Crystallization morphology

Electron diffraction and dark-field electron microscopy showed structure of the crystallized MBF60 to consist of a very fine (approx. 1 nm) eutectoid structure of nickel and Ni_3P. This differed considerably from that of the quenched-in crystals, which had an inter-lamellar spacing about 20 times larger.

Annealing using hot-stage TEM showed that all observed crystallization appeared to nucleate on the surface of quenched-in crystals, growth starting after an incubation time (Fig. 2). Later growth involved the dominance of grains of preferred orientation, resulting in an overall increase in grain size.

The growth of a new crystalline phase on the surface of quenched-in crystals was not detected until after approx. 10% of the time required for complete crystallization (Fig. 3). This incubation time was found to be consistent over a range of temperatures, as detected by optical metallography and hot-stage TEM.

Optical micrographs of partially crystallized glass revealed that crystallization also occurred from apparently homogeneous nuclei. This was not observed in TEM specimens, probably because of the specimen preparation technique resulting in the most thinning occurring around quenched-in crystals.

Similar crystallization morphologies have been reported for other amorphous metal systems. Von Heimendahl [27] reported that in two Fe–Ni–P–B

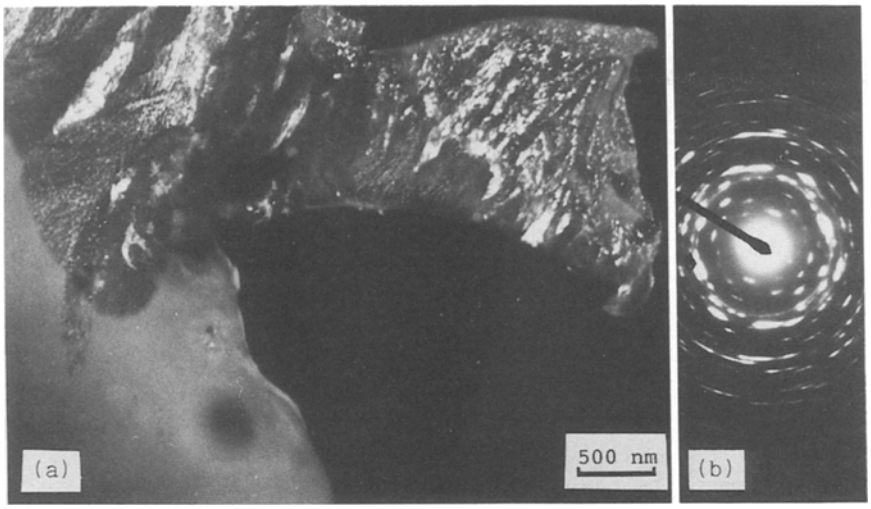

Figure 2 (a) TEM dark-field micrograph (nickel spot) showing crystallization product (left) growing from the edge of a quenched-in crystal (right) in a specimen annealed at 300° C for 32 min. (b) Electron diffraction pattern.

amorphous alloys crystallization occurred after an incubation time, simultaneously on quenched-in crystals and in the bulk of the glass. A similar result was found by Dey and Bannerjee [28, 29] for the crystallization of a Zr–Fe alloy.

Zuercher and Morris [30] took great care to minimize surface and bulk inhomogeneous nucleation sites in an Ni–Si–B alloy. Despite this, simultaneous nucleation at the surface and in the bulk was observed during crystallization at 400° C. At higher temperatures (470° C) bulk nucleation was dominant. Gibson and Delamore [31] found that in some alloys such surface crystallization was independent of defects left over from the melt spinning process. After removal of the surface by grinding, simultaneous nucleation of the (new) surface and in the bulk still occurred.

4.2. Thermal stability

4.2.1. Isothermal crystallization

The thermal stability (TTT curve) was estimated directly from DTA and isothermal annealing tests. Corrections were applied to account for warm-up times before isothermal conditions were established. Similarly, such corrections were applied to the results of DTA runs.

A portion of the TTT diagram for amorphous Ni–11 wt % P metallic glass was evaluated and is shown in Fig. 4. These points represent the time/temperature after which 50 vol% of the material has crystallized. Fig. 5 shows that this compares favourably with the TTT curves determined by Naka *et al.* [10] and Bergmann and Fritsch [17] for the same material. The curves of Bergmann and Fritsch were based on data obtained by DTA, DSC and optical metallography methods and on the observation of the cooling rate achieved during the laser glazing of $Ni_{80}P_{20}$. The curve published by Naka *et al.* is calculated from a theoretically derived equation for the critical cooling rate for glass formation.

If a plot of (1/temp.) against log (time) is a straight line (Fig. 6), the activation energy for crystallization can be estimated as suggested by Chen [6]. The time–temperature dependence has the form

$$1/t = Ae^{Q/RT} \quad (2)$$

where t = crystallization time at temperature T,

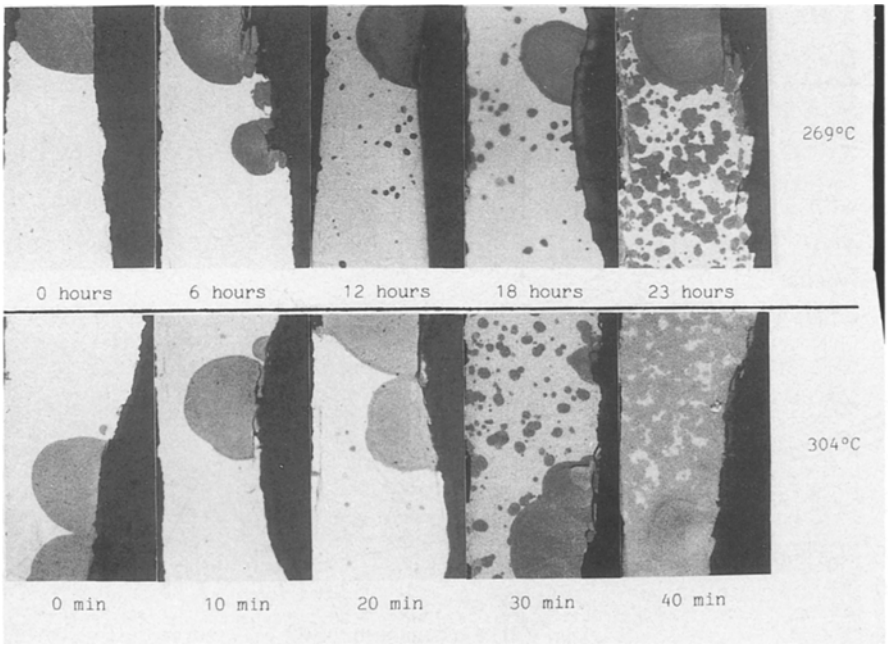

Figure 3 Optical metallographs of partially crystallized metallic glass. Annealing was performed at 269° C (top) and at 304° C (bottom).

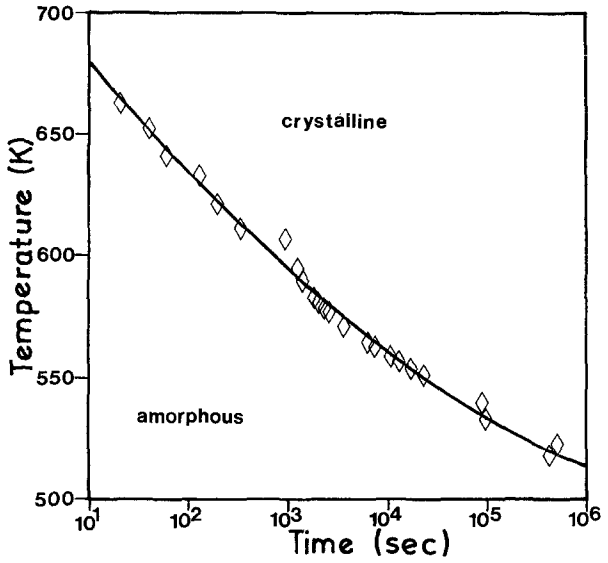

Figure 4 Portion of the TTT curve for the 50 vol % crystallization of the metallic metallic glass MBF60.

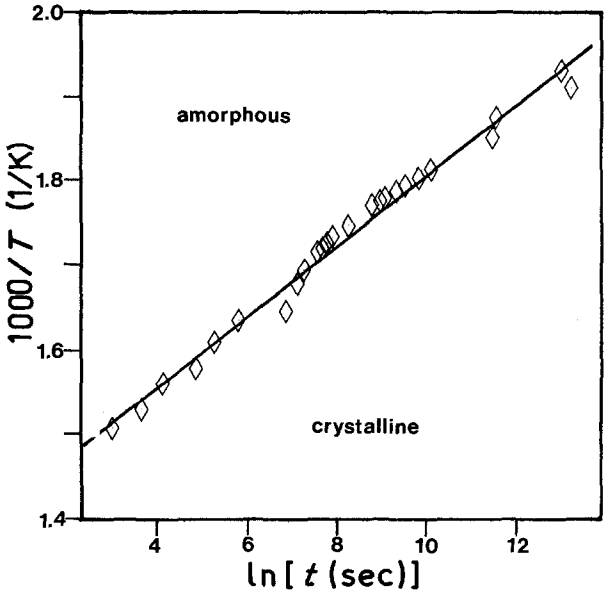

Figure 6 TTT data plotted as $1/T$ against log (time).

A = constant and Q = activation energy for crystallization. For the data of Fig. 6, activation energy equals 256 ± 5 kJ mol^{-1} with a pre-exponential factor of 7.97 × 10^{19} sec^{-1}. This is similar to the result of Criado *et al.* [4], being 283 ± 5 kJ mol^{-1} for a $Ni_{89}P_{11}C$ glass and Von Heimendahl's value of 270 kJ mol^{-1} for the Fe–B glass 2826A [32].

4.2.2. Non-isothermal crystallization

The activation energy for crystallization can be determined directly from DTA data by applying a number of methods based on various models. One is Kissinger's "peak shift method" [3]. In this method, a plot of (T^2/heating rate) against log (time) should yield a straight line. The equation is

$$T^2/\dot{T} = Ae^{-Q/RT} \quad (3)$$

where $\dot{T}$ = heating rate in K sec^{-1}. Peak shift data are plotted in Fig. 7 and yield an activation energy of 226 kJ mol^{-1}.

Other methods of determining the activation energy from DTA curves have been reviewed by Wolny *et al.* [3]. The Augus–Bennett equation

$$(T/\dot{T}) = Ae^{-Q/RT} \quad (4)$$

and the Takhor equation

$$(1/\dot{T}) = Ae^{-Q/RT} \quad (5)$$

are similar to the peak shift equation but yield slightly higher values of activation energy (231 and 236 kJ mol^{-1}, respectively). The Takhor equation is effectively the same as that used in the calculation of thermal stability from DTA data in this work (Fig. 4), only without the corrections for heating rate.

4.3. Incubation times and nucleation rates

The activation energies for incubation time (the time it takes before either crystalline nuclei start to form or quenched-in crystals begin to grow) and nucleation rate (of nuclei formed after the incubation time) were calculated for comparison. The incubation times were

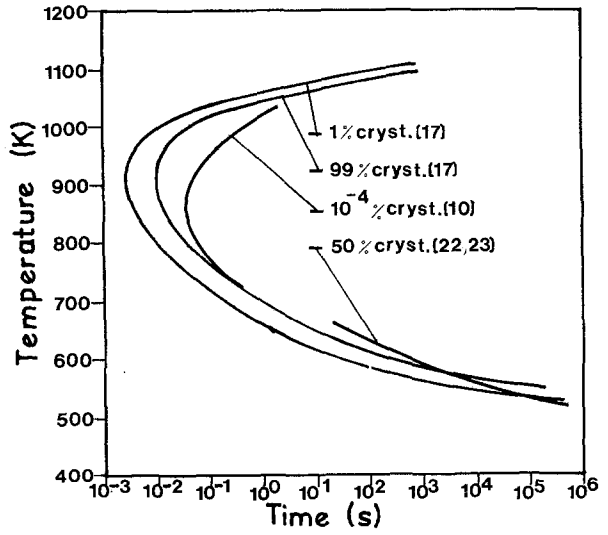

Figure 5 TTT curves for Ni–P metallic glass.

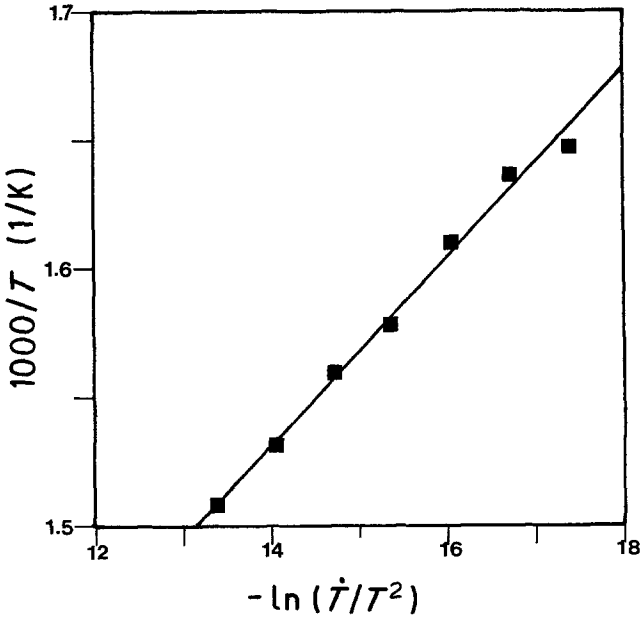

Figure 7 DTA data plotted for the peak shift method.

TABLE I Summary of activation energies for metallic glass*

Model/equation	Data	Q (kJ mol^{-1})	Pre-exponential factor
Peak shift/Kissinger†	DTA	226 ± 15	9.12×10^{11} sec^{-1} K^{-1}
Augis–Bennett†	DTA	231 ± 10	1.57×10^{15} sec^{-1}
Takhor†	DTA	236 ± 10	2.70×10^{18} sec^{-1} K
Crystallization	Isothermal	256 ± 5	7.97×10^{14} sec^{-1}
Growth rate	Isothermal	246 ± 30	2.61×10^{13} sec^{-1} m
Incubation time	Isothermal	185 ± 30	1.13×10^{14} sec^{-1}
Nucleation rate	Isothermal	231 ± 50	5.59×10^{19} sec^{-1}

*Avrami exponent: approx. 1 to 2.
†These results are related as described in the text.

calculated by fitting a straight line to plots of log $(1/t)$ against $1/T$ as in Fig. 8.

The activation energy for nucleation was estimated by plotting nucleation rate against inverse temperature for two temperatures (267 and 301° C). As can be seen from Table I, the activation energy so determined (231 kJ mol^{-1}) was well within the range of the other energies for growth and crystallization.

4.4. Crystallization kinetics

The activation energy for the growth of eutectic crystals was estimated from the temperature dependence of growth rate by the equation used by Koster [25]:

$$U = U_0 e^{-Q/RT} \quad (6)$$

where U = growth rate at temperature. T (m sec^{-1}), U_0 = constant (m sec^{-1}), Q = activation energy for growth (J mol^{-1}), T = temperature (K) and R = 8.314 kJ mol^{-1} K^{-1}.

Our growth rate data have been analysed using this equation (Fig. 9). The higher growth rate found in TEM hot-stage results may indicate enchanced diffusion due to the thinness of the TEM specimen (surface diffusion) and/or enchanced thermal activation as provided by the electron beam. The reduced pressure in the TEM could also contribute to this, as high pressures have been found to retard crystallization in Fe–B alloys [33].

Because of these considerations, as well as the difficulty in establishing isothermal conditions and measuring temperature accurately in the TEM hot stage, the activation energy for growth was determined from data obtained by metallographic methods only. The activation energy was 246 ± 30 kJ mol^{-1}, with $U_0 = 2.605 \times 10^{13}$ m sec^{-1}. This activation energy is comparable to Koster's value of 253 kJ mol^{-1} for an $Fe_{40}Ni_{40}B_{20}$ glass using the same method [2].

The kinetics of nucleation and growth are often described [34] by the Johnson–Mehl–Kolmogorov–Avrami (JMKA) equation

$$x(t) = 1 - \exp[-k(t - t_i)^n] \quad (7)$$

where $x(t)$ = fraction crystallized at time t, t_i = incubation time (before growth) (sec), k = rate constant and n = a constant sometimes known as the Avrami exponent. For isothermal experiments, Equation 7 can be transformed into

$$\ln[\ln(1/1-x)] = \ln k + n \ln(t - t_i) \quad (8)$$

Plotting data in this form (Fig. 10) allows the determination of the constants k and n by linear regression. This was done for two temperatures, using times and crystallized fractions determined by optical metallography. The results are shown in Table II. The data are given elsewhere [22, 23].

These values of the Avrami exponent are comparable with the results of Budurov *et al.* [34] who determined Avrami exponents for an $Fe_{80}B_{20}$ metallic glass. Exponents determined for a number of temperatures between 613 and 653 K varied from 1.50 to 2.57. Values of ln$k$ were similar. In the interpretation of the JMKA equation, particular values of the Avrami exponent indicate particular modes of growth [34].

The experimental values of n = 1 to 2 indicate that simultaneous growth on quenched-in crystals and the formation and growth of eutectoid grains within the amorphous phase could be occurring. This is consistent with the observations of Herold and Koster [35], and with the structures seen in Fig. 11.

4.5. Summary of activation energies

The activation energies for crystallization of the metallic glass were calculated using crystallization temperatures determined at heating rates ranging from 0.625 to 40 K min^{-1}. The activation energies using the three DTA methods as well as energies for growth, nucleation, incubation and overall crystallization are summarised in Table I.

The activation energy for crystallization is based on the time taken for 50 vol % of the material to crystallize. This time includes any incubation time (before growth starts) and the time taken for growth to the required crystallized fraction. The activation energy for growth is based on the actual growth rates, regardless of any overall crystallization or incubation times.

A re-examination of the equations for non-iso-

TABLE II Parameters of the JMKA determined from experimental results

Temperature (K)	Incubation time (sec)	ln k	Avrami exponent, n	Rate constant, k
540	8400	−25.77	2.2	18.7×10^{-10}
574	1500	−10.37	1.0	30.8×10^{-5}

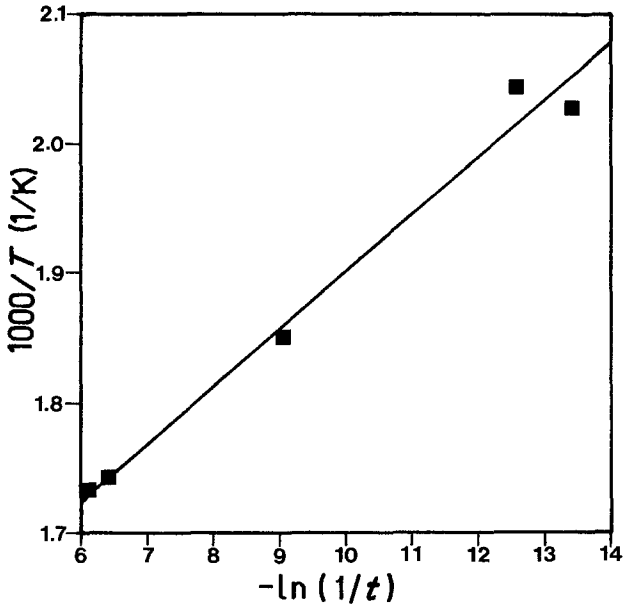

Figure 8 Incubation time data plotted for activation energy.

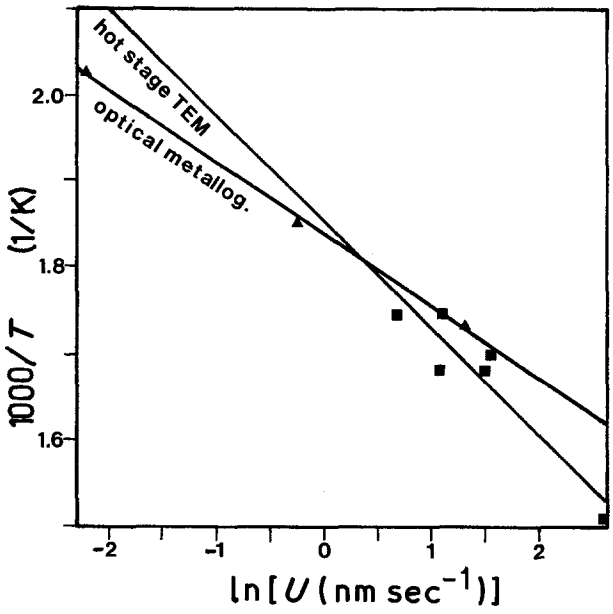

Figure 9 Plot of $1/T$ against log (growth rate).

thermal crystallization will reveal that the right-hand side (RHS) of the Augus–Bennett equation is the derivative (with respect to temperature) of the RHS of the Kissinger equation and that the RHS of the Takhor equation is the derivative of the RHS of the Augus–Bennett equation. Consequently all these results are related. Wolny *et al.* [3] have explained that the Kissinger equation yields the activation energy of the first stage of crystallization, and is thus the best approximation of activation energy measured by isothermal methods. The other equations are derived by making progressively more approximations about the crystallization process.

5. Discussion

The observation that growth on quenched-in crystals does not begin until nucleation and growth of possibly homogeneously nucleated crystals also begins is a phenomenon that has perplexed some workers [28, 29]. Bergmann and Fritsch [17] suggest that quenched-in crystals would cause a lowering of the TTT curve at lower temperatures, implying that growth on quenched-in crystals will begin just prior to homogeneous nucleation. Koster and Herold [36] realized that the energy of an amorphous–crystalline interface is relatively low and therefore heterogeneous nucleation at surfaces or interfaces is not as common as in crystalline materials. Therefore above T_g they did not expect the TTT behaviour to be affected markedly by heterogeneous nucleation.

In this work an incubation time preceding crystallization was found that was approximately the same for the start of growth of quenched-in crystals and the start of homogeneous nucleation. One explanation is that all growth was on quenched-in crystals, many being too small to be resolved. However, new crystals appear over time suggesting that nucleation is occurring. Also the Avrami exponent implies that growth of quenched-in crystals and nucleation are occurring simultaneously. Furthermore, the TTT curve obtained experimentally matches that predicted by Naka *et al.* [10], whose model was based on homogeneous nucleation from the liquid.

The above implies that the activation energy for the start of growth on quenched-in crystals is the same as that for nucleation. This was calculated to be the case (Table I), indicating that both processes are controlled by the same mechanism. In fact, the activation energies of nucleation, growth and crystallization were all similar. The most likely mechanism is diffusion of atoms as long-range diffusion is necessary to form the eutectic structure on crystallization.

This negates the concept of an activation energy for nucleation as it is known for normal freezing at temperatures above the nose of the TTT curve. Above the nose the activation energy is that required to create an interface between the crystal and the liquid. Below the nose the chemical driving force for crystallization is so high that any barrier to nucleation becomes insignificant compared to the difficulty of moving atoms.

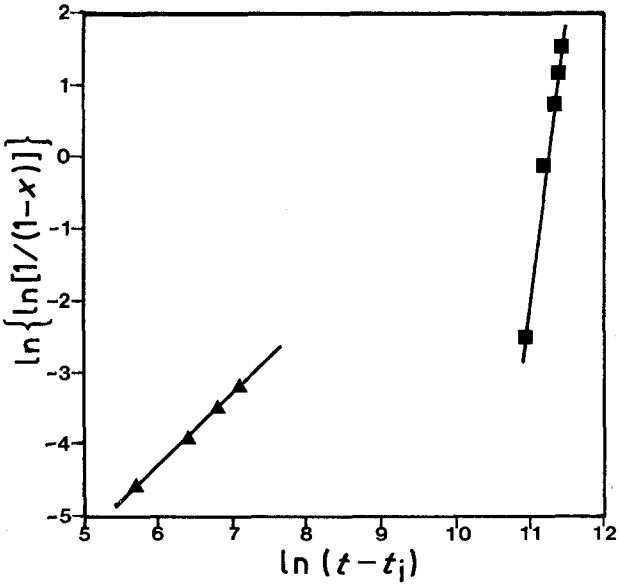

Figure 10 Plots of crystallization fitted to the JMKA equation: (■) 540 K, (▲) 574 K.

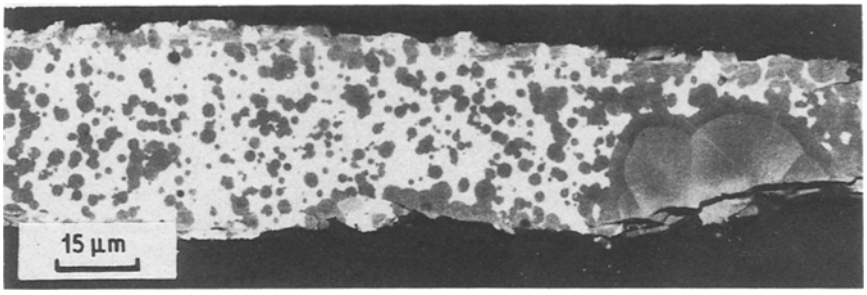

Figure 11 Crystallization of the metallic glass. Specimen annealed at 304° C for 35 min. Optical micrograph.

Diffusion activation does not explain the incubation time for growth on to quenched-in crystals, because once growth begins it continues without the need for further incubation. Since this incubation time is consistently the same fraction of the crystallization time for a number of temperatures (Fig. 4), it follows that the incubation process is diffusion-controlled and is therefore not an athermal transformation.

This would be consistent with the time lag observed in the crystallization or more conventional eutectic structures, which results in the reorganization of the crystalline interface to accommodate the appropriate lamellar spacing [37]. However, it is then a coincidence that this time is similar to that for homogeneous nucleation.

A more likely explanation is that the supercooled liquid has difficulty in transforming directly to crystalline phases and must rearrange to some extent to become closer in structure. This process would be equivalent to relaxation [13]. Regions of glass produced at the fastest cooling rates will have a structure corresponding to a higher temperature, and thus need more rearranging to obtain the equilibrium liquid structure for the temperature of anneal. The liquid's free energy will be lowered by this rearrangement by lowering the internal energy of the system. Once liquid equilibrium is attained, further lowering of free energy requires crystallization.

It is therefore expected that growth or nucleation will occur first where the liquid has experienced the slowest cooling rate. In the alloy that region is the glass next to the large quenched-in crystals (therefore giving the appearance of epitaxial nucleation at the crystalline–liquid interface). Further nuclei should appear in faster cooling rate regions as time progesses. Any observed nucleation rate would be a composite of overlapping nucleation rates. Therefore measurement of the activation energy for nucleation is not valid as it will reflect that for diffusion generally. The measured pre-exponential factor also has no relevant meaning.

The incubation time simply reflects ordering of atoms in the liquid to form a relaxed or equilibrium structure before crystallization takes place. Therefore it is a part of a continuum where the free energy is continually lowered without activation barriers existing between steps. The proportion of the time to complete crystallization given to the incubation period was a consistent 10% regardless of temperature. If there was a nucleation barrier this proportion should be less at lower temperatures.

Given this constant proportionality, the activation energy for nucleation would be expected to be the same as that for crystal growth, i.e. the diffusion of atoms in the supercooled liquid.

Nucleation at annealing temperatures would correspond to the creation of a cluster in the liquid whose structure is similar to the crystalline form of one of the phases. The interfacial energy is negligible compared to the chemical driving force, therefore cluster formation will lead directly to a stable nucleus with the activation energy corresponding to the diffusion of atoms necessary to create a cluster of the correct composition and structural arrangement. Cluster formation is a random process but clearly clusters of the correct type do not exist in higher-temperature liquids, otherwise growth will begin as soon as atoms can diffuse. The structure of the liquid must change to allow the cluster to exist.

So far this discussion has been concerned with two-phase crystallization products. In the case of polymorphic transformation, the crystalline phase has the same composition as the amorphous phase. Where crystallization can occur without composition change only a topological rearrangement of atoms is necessary, and clusters of the correct structure are probably present [38]. Any incubation time would be very short and probably not observed experimentally. Crystallization will occur at or near T_g. This is observed for Cu–Ti alloys [39]. In such cases single-phase crystallization products occur for all compositions [40].

Given the supporting data of similar activation energies for each stage of crystallization, the Avrami exponent and the microstructural observations, diffusion and short-range rearrangement of atoms (relaxation) are the rate-controlling steps throughout. This is in keeping with accepted phase transformation theory, where above the nose of the TTT curve the activation energy is controlled by the need to form stable nuclei (by overcoming the increase in free energy caused by the creation of an interface) and below the nose the difficulty of atoms to diffuse controls the transformation.

6. Conclusions

Amorphous $Ni_{81}P_{19}$ metallic glass crystallizes by a eutectoid reaction to nickel and Ni_3P. No intermediate phases were observed. Crystallization occurred on quenched-in crystals of Ni–Ni_3P eutectic and also appeared to nucleate homogeneously in the glass, with both exhibiting a similar incubation time.

Growth kinetics were modelled to the Johnson–Mehl–Kolmogorov–Avrami equation and a value of between 1 and 2 was obtained for the Avrami

exponent, indicating the simultaneous growth of quenched-in crystals and the homogeneous formation of eutectoid grains within the amorphous phase, and thus supporting the microstructural observations.

The TTT curve was found to agree well with those already published for Ni–P amorphous alloys. The activation energies for nucleation, growth and crystallization were calculated by various methods and were found to be in the range of 210 to 256 kJ mol^{-1}.

All processes have similar activation energies, indicating that diffusion of atoms is rate-controlling. The incubation period reflects the reordering of supercooled liquid to its equilibrium structure, and the composition to that of at least one of the crystallizing phases.

Calculation of the activation energy of nucleation is shown to be invalid for Ni–P glass below the nose of the TTT curve. It is suggested that there is a negligible activation barrier to nucleation at these temperatures, in accordance with the accepted theory developed for the diffusional phase.

Acknowledgements

EDS analysis was carried out at BHP Melbourne Research Labs with the assistance of Dr Harry Buskes. All other experimental work was undertaken in the Departments of Applied Physics and Metallurgy and Mining, RMIT. J. H. H.-H. acknowledges the financial support of the John Storey Jnr Memorial Trust Committee and the RMIT Research Committee.

References

1. K. MULLER and M. Von HEIMENDAHL, *J. Mater. Sci.* **17** (1982) 2525.
2. U. KOSTER, *Z. Metallkde* **75** (1984) 691.
3. J. WOLNY, J. SOLTYS and R. KOKOSZKA, *J. Non. Cryst. Solids* **91** (1987) 209.
4. A. CRIADO *et al.*, *Mater. Lett.* **5** (1987) 182.
5. T. R. ANANTHARAMAN, in "Metallic Glasses Production, Properties and Applications", edited by T. R. Anantharaman (Trans Tech, Switzerland, 1984) pp. 1–29.
6. H. S. CHEN, *Appl. Phys. Lett.* **29** (1976) 12.
7. M. TAKASHI, M. KOSHIMURA and T. ABAZUKA, *Jpn J. Appl. Phys.* **20** (1981) 1821.
8. N. DECRISTOFARO, A. FREILICH and G. FISH, *J. Mater. Sci.* **17** (1982) 2365.
9. H. S. CHEN, *Acta Metall.* **24** (1976) 153.
10. M. NAKA, A. INOUE and T. MASUMOTO, *Sci. Rep. Res. Inst. Tohoku Univ. A Series* **29** (1981) 184.
11. W. OZGOWICZ *et al.*, *Scripta Metall.* **17** (1983) 295.
12. R. L. FREED and J. B. VANDER-SANDE, *J. Non-Cryst Solids* **27** (1978) 9.
13. H. S. CHEN, *Rep. Progr. Phys.* **43** (1980) 353.
14. I. BAKONYI *et al.*, *Z. Metallkde* **77** (1986) 425.
15. U. PITTERMANN and S. RIPPER, in "Rapidly Quenched Metals", edited by S. Steeb and H. Warlimont (Elsevier, Amsterdam, 1985) p. 385.
16. W. DING *et al.*, *Scripta Metall.* **21** (1987) 1685.
17. H. W. BERGMANN and H. U. FRITSCH, in "Rapidly Solidified Metastable Materials", edited by B. H. Kear and W. C. Giessen, Metals Research Society Symposia Proceedings Vol. 28 (North-Holland, New York, 1984) p. 3.
18. K. MASUI, S. MARUNO and T. YAMADA, *J. Jpn Inst. Met.* **41** (1977) 1130.
19. *Idem, ibid.* **44** (1980) 124.
20. E. VAFAEI-MAKHSOS, *J. Appl. Phys.* **51** (1980) 6366.
21. K. H. KUO *et al.*, *Phil. Mag.* **51** (1985) 205.
22. J. HAMLYN-HARRIS, Masters degree thesis, Royal Melbourne Institute of Technology (1986).
23. J. HAMLYN-HARRIS, D. H. StJOHN and D. K. SOOD, *MRS Proc.* **51** (1985) 497.
24. C. M. ADAM, Personal Communication.
25. U. KOSTER, *MRS Proc.* **28** (1984) 175.
26. D. G. MORRIS, *Met. Sci.* **16** (1982) 457.
27. M. Von HEIMENDAHL, in "Rapidly Quenched Metals", edited by S. Steeb and H. Warlimont (Elsevier, Amsterdam, 1985) p. 279.
28. G. K. DEY and S. BANNERJEE, *Meter. Sci. Engng* **76** (1985) 127.
29. *Idem, ibid.* **73** (1985) 185.
30. M. -H. ZUERCHER and D. G. MORRIS, *J. Mater. Sci.* **23** (1988) 515.
31. M. A. GIBSON and G. W. DELAMORE, *ibid.* **22** (1987) 4550.
32. M. Von HEIMENDAHL, *J. Mater. Sci. Lett.* **2** (1983) 796.
33. W. -K. WANG, H. IWASAKI and K. FUKAMICHI, *J. Mater. Sci.* **15** (1980) 2701.
34. S. BUDUROV, T. SPASSOV and T. MARKOV, *ibid.* **21** (1986) 2553.
35. U. HEROLD and U. KOSTER, in "Rapidly Quenched Metals III", Vol. I, edited by B. Cantor (Metals Society, London, 1978) p. 281.
36. U. KOSTER and U. HEROLD, in "Glassy Metals I", Topics in Applied Physics Vol. 46, edited by H. -J. Guntherodt and H. Beck (Springer, Berlin, 1981) p. 225.
37. R. ELLIOT, in "Eutectic Solidification Processing" (Butterworths, London, 1983) pp. 67–68.
38. P. DUWEZ, *ASM Trans.* **60** (1967) 607.
39. T. B. MASSALSKI and C. G. WOYCHIK, *Acta Metall.* **33** (1985) 1873.
40. D. H. StJOHN, *Metall. Trans. A.* "Freezing Diagrams Pt III, Comparison with Experimental Observation and Relevance to Crystallization of Metallic Glass." In press.

Received 27 October 1988
and accepted 14 April 1989